KSCE Journal of Civil Engineering (2021) 25(12):4897-4912
DOI 10.1007/s12205-021-0618-4

pISSN 1226-7988, eISSN 1976-3808
www.springer.com/12205

Tunnel Engineering

Decoupling Analysis of Interaction between Tunnel Surrounding Rock and Support in Xigeda Formation Strata

Ping Zhou[a,b], **Feicong Zhou**[a,b], **Jiayong Lin**[a,b], **Jinyi Li**[a,b], **Yifan Jiang**[a,b], **Bao Yang**[c], **and Zhijie Wang**[a,b]

[a]*Key Laboratory of Transportation Tunnel Engineering, Ministry of Education, Southwest Jiaotong University, Chengdu 610031, China*
[b]*School of Civil Engineering, Southwest Jiaotong University, Chengdu 610031, China*
[c]*CREEC (Chongqing) Survey, Design and Research Co., Ltd., Chongqing 401121, China*

ARTICLE HISTORY

Received 12 April 2021
Revised 8 June 2021
Accepted 21 June 2021
Published Online 15 August 2021

KEYWORDS

Xigeda formation strata
Rock-support characteristics
Decoupling analysis
Dilatancy
Shotcrete timeliness

ABSTRACT

The Xigeda Formation has the characteristics of poor cementation, variable structure, and softening in water. It is prone to lead to failure of the initial support structures, arch collapse, and even roof fall. The key to the problem lies in the exploration of the interaction between surrounding rock and support. Therefore, based on the constraint loss theory of the tunnel face space effect, this paper constructively introduces multiple dependent variables, including the intermediate principal stress, the dilatancy of the surrounding rock, the timeliness of the shotcrete support stiffness, and the water content of the Xigeda formation, to decouple the whole process of the interaction between the surrounding rock and support, and discusses the influence of each variable. The research results show that: i) there is a critical support point in the tunnel under the influence of the unified strength theoretical parameter b and water content, and when the unified strength theoretical parameter *b* is constant, the critical distance of the support will decrease with the increase of the water content; ii) from the perspective of deformation control, the stress of support structure will increase with the increase of dilatancy angle of Xigeda surrounding rock; iii) considering the hardening characteristics of shotcrete, the initial support stiffness of Xigeda tunnel increases nonlinearly, and the whole process of stress and deformation can be divided into four stages; iv) the combined support structure of section steel and grille has little difference in the deformation control effect of the surrounding rock and the stress of the support structure, but the combined support structure of the grille steel frame is more sensitive to the hardening parameters.

1. Introduction

With the rapid economic growth of cities in western China, the transportation construction in the western mountain area has ushered in an unprecedented development, the most typical of which is the Chengdu-Kunming railway expansion and reconstruction project (Chengdu-Kunming double track). There is various unfavorable geology along the Chengdu-Kunming railway, the most famous of which is the Xigeda formation. The Xigeda formation, consisting of siltstone and clay rock, is a famous half-diagenesis formed in different fluvio-lacustrine deposits environments in southwestern China, with the characteristics of poor cementation, variable structure, and softening in water. There are a large number of tunnels passing through the Xigeda formation in the Chengdu-Kunming double track (see Fig. 1), Chengdu Kunming railway is the most famous railway line in Southwest China. Most of the tunnels pass through Xigeda formation. Taking the mileage section from Miyi to Panzhihua as an example, there are 18 tunnels among which, 10 tunnels cross Xigeda stratum, with a total length of 10.4 km, and the engineering strength of the surrounding rock is acceptable in an environment without water. However, under the double effects of groundwater and excavation disturbance, the strength and stability of the surrounding rock of the Xigeda formation decreases sharply due

CORRESPONDENCE Ping Zhou ZhouPing1896@my.swjtu.edu.cn Key Laboratory of Transportation Tunnel Engineering, Ministry of Education, Southwest Jiaotong University, Chengdu 610031, China; School of Civil Engineering, Southwest Jiaotong University, Chengdu 610031, China

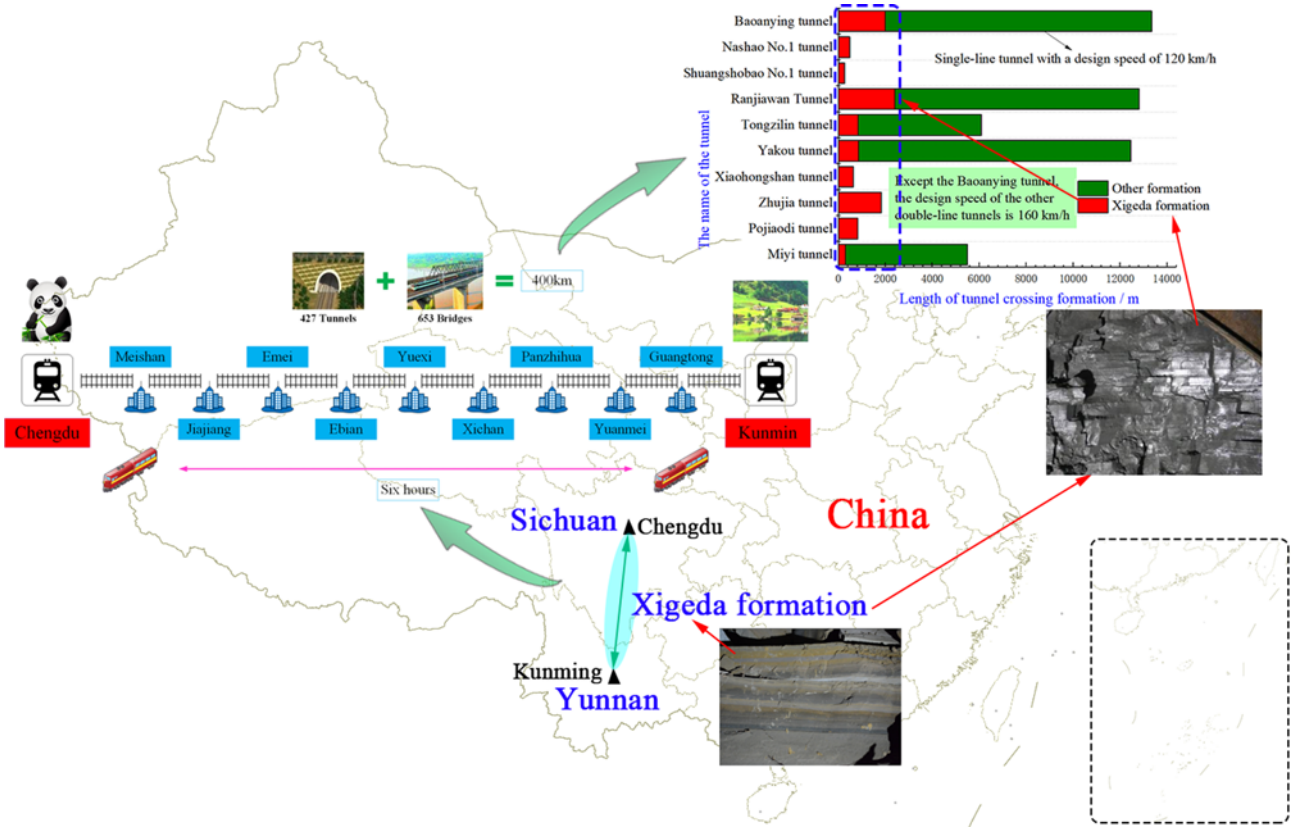

Fig. 1. Xigeda Formation Tunnel Project (Chengdu-Kunming double track)

Fig. 2. Tunnel Engineering Disaster in Xigeda Formation: (a) Crashing Failure of Primary Support, (b) The Mudding of the Tunnel Face, (c) Tunnel Entrance Collapse, (d) Vault Collapse, (e) Steel Frame Deformation, (f) Ground Surface Collapse

to the increase of water content, which is prone to the occurrence of engineering disasters during tunnel construction, such as the shotcrete cracked and dropped, steel frame deformation, collapse, even roof fall (see Fig. 2). Fig. 2(a) shows the partially mudding of the surrounding rock in Xigeda tunnel. Fig. 2(b) shows the mudding of the tunnel face. Fig. 2(c) shows the collapse

phenomenon of Xigeda tunnel. Fig. 2(d) shows the vault collapse of Xigeda tunnel. Fig. 2(e) shows the large deformation of the steel frame. Fig. 2(f) shows the surface collapse. Therefore, the special hydraulic properties of the Xigeda formation aggravate the complexity of the interaction between surrounding rock and support.

The traditional convergence-confinement method takes the intersection of the ground reaction curve and the support reaction curve as the equilibrium state of the surrounding rock and the support, based on which, a large number of studies have been conducted to investigate the support parameter design (Carranza-Torres and Fairhurst, 2000; Lee and Pietruszczak, 2008; Gschwandtner and Galler, 2012; Cui et al., 2014; Shishegaran et al., 2020a; Shishegaran et al., 2020b; Naghsh et al., 2021; Shishegaran et al., 2021a; Shishegaran et al., 2021b). Lee and Pietruszczak (2008) first layered the plastic zone of the surrounding rock according to the radial stress, then solved the stress and strain of each layer by the finite difference method, and finally obtained the plastic radius of the surrounding rock and the displacement of the tunnel wall through iterative calculation. In order to more reasonably reflect the nonlinear dilatancy of rock mass, Cui et al. (2014) considered the nonlinear characteristics of the dilatancy angle of surrounding rock changing with the increase of plastic strain, and compared it with the constant dilatancy angle model. Gschwandtner and Galler (2012) considered the adaptability of the reinforcement effect of the system bolt and the timeliness of shotcrete in the convergence-confinement method of surrounding rock.

However, these studies adopt the linear Mohr-Couloumb criterion and the nonlinear Hoek-Brown criterion without considering the effect of intermediate principal stress. With the research on the effect of intermediate principal stress, scholars have found that ignoring the effect of intermediate principal stress will lead to failure to fully utilize the strength potential of the surrounding rock (Jin et al., 2019; Khalid et al., 2019; Kwong et al., 2019; Shishegaran et al., 2019; Es-Haghi et al., 2020; Mortazavi et al., 2020; Shishegaran et al., 2020c). In addition, due to the spatial effect of the tunnel face, the stress release of the surrounding rock is not complete, which affects the force of the entire support system (Unlu and Gercek, 2003; Alejano et al., 2012). Therefore, it is very important to determine the evolution law of stress release during the excavation.

By reviewing literatures, it is found that there are many limitations existing in the traditional convergence-confinement method. It can neither well show the significant spatial effect of tunnel excavation, nor can it clearly explain the interaction mechanism between surrounding rock and support. Compared with the traditional convergence-confinement method, the two-stage analysis method is more reasonable, which regards the spatial effect of the tunnel face as a virtual support pressure (Osgoui and Oreste, 2009; Fahimifar and Ranjbarnia, 2009; Carranza-Torres et al., 2013; Cui et al., 2015).

This paper proposes a numerical method for solving the interaction process between the surrounding rock and the support of the tunnel, which constructively considers the intermediate principal stress, the dilatancy of the surrounding rock, the timeliness of the shotcrete support stiffness, and the water content of the Xigeda formation at the same time. Furthermore, taking the shale sandstone Xigeda formation tunnel as the research object, the interaction between surrounding rock and support is decoupled, which means to decompose the support force acting on the surrounding rock into the virtual support pressure and the support reaction provided by the support structure. In addition, systemic parametric analyses are performed to explore and discuss the influences of various factors on the variation of surrounding rock deformation and support stress, including the unified strength theoretical parameter, dilatancy angle, support stiffness, supporting opportunity, hardening properties and water content. The research results in this paper can provide a theoretical basis for excavation and support in the Xigeda formation.

2. Tunnel Excavation Mechanics Model and Basic Assumptions Based on the Spatial Effect of the Tunnel Face

2.1 The Whole Process of Interaction between the Surrounding Rock and Support during Tunnel Construction

The spatial constraint effect of the tunnel face can be regarded as the virtual support pressure applied to the inner wall of the tunnel. As the distance from the tunnel face increases, the spatial constraint effect of the tunnel face keeps losing, and the virtual support pressure also decreases, then the release rate of surrounding rock stress gradually increases. It can be seen that by quantifying the spatial effect of the tunnel face into a virtual support pressure, the quantitative analysis of the spatial constraint effect of the tunnel face can be realized, and the three-dimensional tunnel problems can be transformed into a plane state for the solution. Based on the constraint principle of the spatial effect of the tunnel face, the relationship between the surrounding rock and the support at different positions can be equivalent to four mechanical models in the longitudinal direction of the tunnel. At the same time, it also represents the 4 stages of the interaction between the surrounding rock and the support of the tunnel. as shown in Fig. 3. Fig. 4 shows mechanical model of circular tunnel, When the tunnel is excavated in the stratum with poor rock mass, the surrounding rock will continue to deform under constant stress after yielding, that is, the rock mass can be regarded as an ideal elastic-plastic body. For the ideal elastic-plastic rock body, the surrounding rock can be divided into two areas. The rock mass near the free face reaches the yield strength to form plastic zone or plastic flow area, and the deep part does not reach the elastic zone of yield strength.

For areas that are not affected by the disturbance of tunnel excavation, such as section $A-A'$, it can be considered that there is a supporting force equivalent to the stress of the original rock acting around the tunnel, and the surrounding rock does not

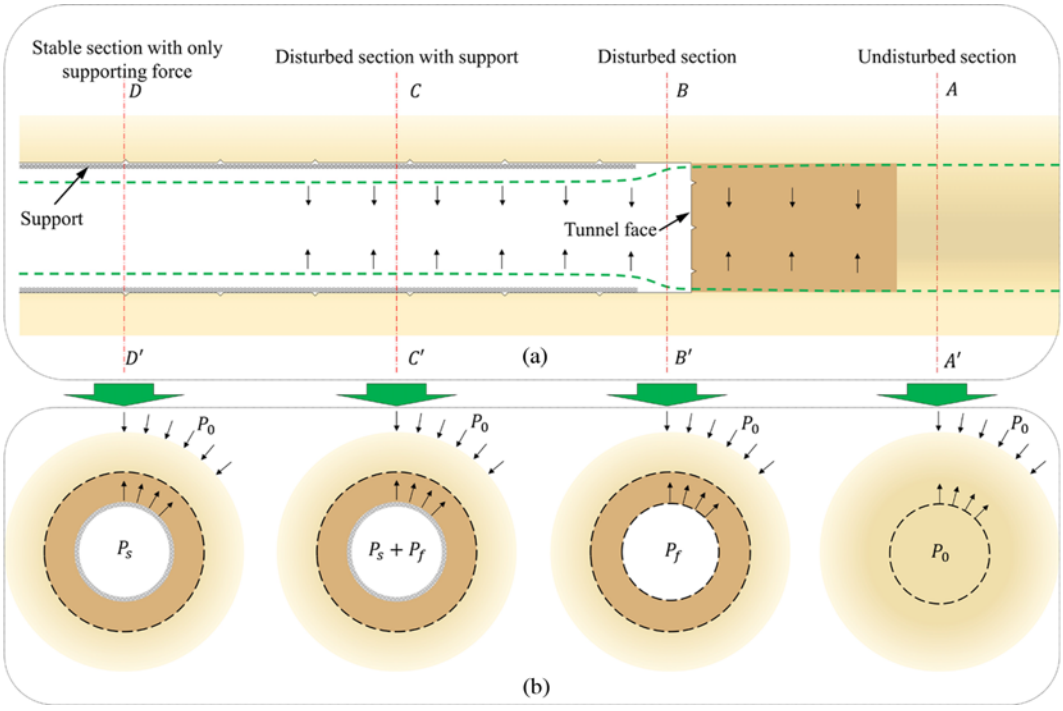

Fig. 3. The Complete process of Interaction between Surrounding Rock and Support: (a) Tunnel Longitudinal Section, (b) The relationship between Surrounding Rock and Supporting Force on Different Cross-Sections of Tunnel

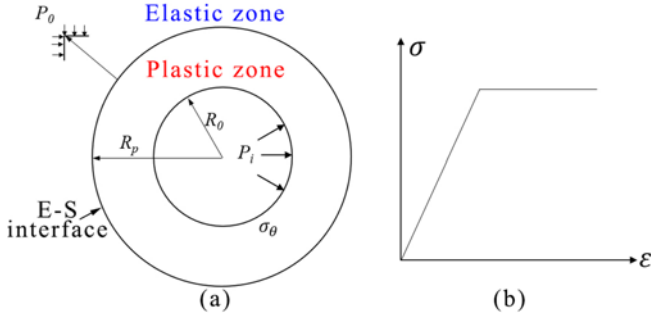

Fig. 4. Mechanical Model of Circular Tunnel: (a) Elastoplastic Partition, (b) Stress-Strain Relationship

change in stress and displacement; when artificial support is not applied in the tunnel face, such as section $B-B'$, the stability of the tunnel depends only on the virtual support pressure P_f provided by the spatial effect of the tunnel face; when artificial support is applied, within the effect range of the tunnel face, such as section $C-C'$, the virtual support pressure P_f and the support structure support force P_s act together on the inner wall of the tunnel; as the spatial effect of the tunnel face continues to weaken, the virtual support pressure decreases and the support reaction increases; when the distance is large enough, there is only the support reaction P_s of the support structure.

2.2 Mechanical Model and Yield Criterion of a Circular Tunnel

When the size of the tunnel axis is much larger than the transverse size, the three-dimensional problem can be regarded as a plane strain problem, and the surrounding rock is in an axisymmetric state, so the balance equation and geometric equation are expressed in the cylindrical coordinate system as

$$\frac{d\sigma_r}{dr}+\frac{\sigma_r-\sigma_\theta}{r}=0\,, \tag{1}$$

$$\varepsilon_r=\frac{du}{dr},\ \varepsilon_\theta=\frac{u}{r},\ \varepsilon_z=0\,. \tag{2}$$

When a circular tunnel with a radius of R_0 is excavated in the hydrostatic in-situ stress field P_0, a force of P_i applies to the inner wall, and the plastic radius is R_p, as shown in Fig. 4. Regarding the surrounding rock as a homogeneous and isotropic ideal elastic-plastic body, it obeys the unified yield criterion, the equation is expressed by the internal friction angle φ and cohesive c of the material shear strength parameters as

$$F(\sigma_{ij})=\sigma_\theta-A_{ust}\sigma_r-B_{ust}=0\,, \tag{3}$$

where $A_{ust}=\left[(2+b)+(2+3b)\sin\varphi\right]/\left[(2+b)(1-\sin\varphi)\right]$, $B_{ust}=[4(1+b)c\cos\varphi]/[(2+b)(1-\sin\varphi)]$. The unified theoretical strength parameter b reflects the intermediate principal stress effect of the surrounding rock. The larger the value of b, the more significant the intermediate principal stress effect of the surrounding rock, $0\le b\le 1$.

The relationship between the radial strain and the tangential strain in the plastic zone is obtained by using the non-associated flow law as

$$\varepsilon_r^p+\beta\varepsilon_\theta^p=0\,, \tag{4}$$

where $\beta=\left[(2+b)+(2+3b)\sin\psi\right]/\left[(2+b)(1-\sin\psi)\right]$, ψ is the dilatancy angle of the rock, and is assumed to be a constant value in the plastic zone.

2.3 Coupling Solution of the Virtual Support Pressure

The longitudinal deformation profile of the tunnel reflects the longitudinal distribution of the radial convergence deformation of the surrounding rock under the condition without support, which is the release law of the tunnel displacement under the spatial constraint of the tunnel face, and also reflects the attenuation law of the virtual support pressure provided by the spatial effect of the tunnel face. For the elastic stage, there is a linear relationship between the displacement release rate and the virtual support pressure. However, when the surrounding rock enters the plastic deformation stage, there is a nonlinear relationship between the displacement release rate and the virtual support pressure. Therefore, the change law of the tunnel displacement release rate cannot be completely equal to the change law of the virtual supporting force. It can be obtained from the ground reaction curve that the radial displacement of the surrounding rock can be obtained by knowing the force of the inner wall of the tunnel, and the supporting force applied to the inner wall of the tunnel can also be obtained after the radial displacement of the inner wall of the tunnel is known. Based on this, the coupling solution method of the virtual support pressure can be determined, as shown in Fig. 5.

For a certain location of the tunnel (such as point B), the radial displacement of the inner wall of the tunnel without any support structure is u_b. The relationship between the radial displacement of the tunnel and the support force can be solved to obtain the support force P_b when the radial displacement is u_b, and the support force at this time is provided by the spatial effect of the tunnel face, that is, virtual support pressure $P_b=P_f^b$. This link needs to determine the tunnel displacement release coefficient prediction formula, that is, the LDP curve. The displacement release coefficient based on the largest plastic radius of the surrounding rock comprehensively considers the influence of multiple factors and has a wider scope of application. The displacement equation fitted by N. Vlachopoulos and M. S. Diederichs based on a large number of finite difference method simulation data is expressed as

$$\left.\begin{aligned} u_0^* &= \frac{1}{3}\exp\left(-0.15R^*\right) && (x=0)\\ u^*(x) &= \frac{u(x)}{u_{\max}} = u_0^*\exp\left(x^*\right) && (x\le 0)\\ u^*(x) &= \frac{u(x)}{u_{\max}} = 1-\left(1-u_0^*\right)\exp\left(-\frac{1.5x^*}{R^*}\right) && (x\ge 0) \end{aligned}\right\}, \tag{5}$$

where the radial displacement u^*, plastic radius R^*, and the distance to the tunnel face are all standardized forms, $u(x)$ is the displacement away from the tunnel face x, and $u_{\max}$ is the maximum radial displacement after the ground stress is completely released, u_0^* is the displacement release coefficient at the position of the face; $R^*=R_p^{\max}/R_0$, $R_p^{\max}$ is the plastic radius when the supporting force is zero; $x^*=x/R_0$, R_0 is the excavation radius, x is less than zero refers to the front of the tunnel face, x greater than zero refers to the rear of the tunnel face.

3. Ground Reaction Curve considering Intermediate Principal Stress

The development of the ground reaction curve of the Xigeda formation tunnel involves three processes (see Fig. 6). The AB section represents the elastic stage. At the initial stage of tunnel excavation, the surrounding rock is in the elastic stage, so the AB section is a straight line with elastic behavior on the characteristic

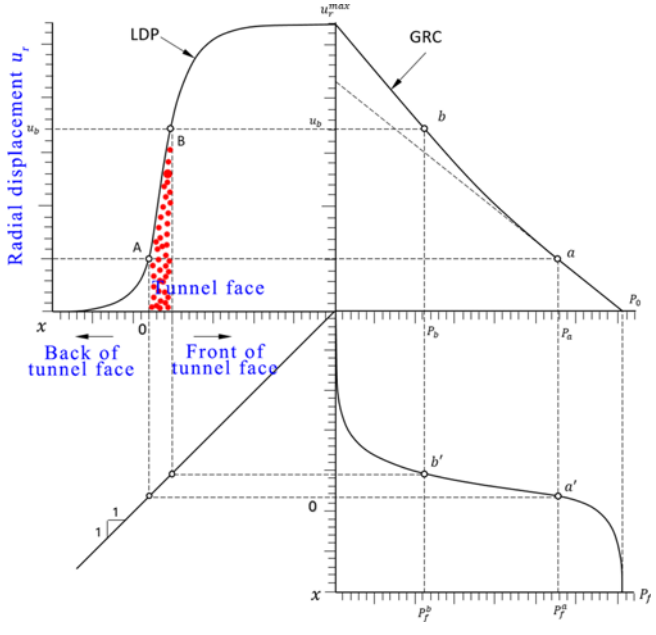

Fig. 5. Coupling Solution of Virtual Support Pressure

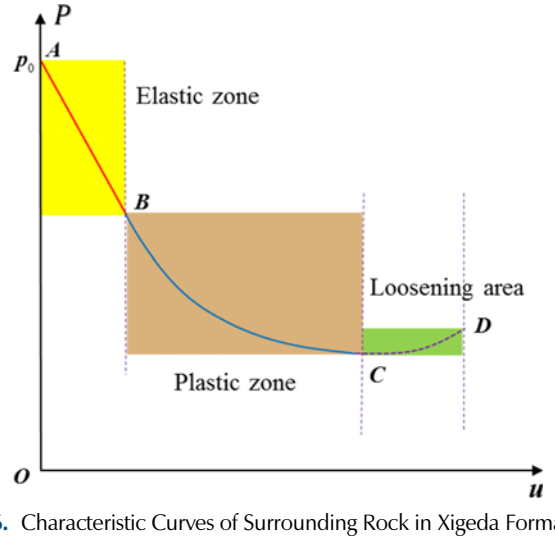

Fig. 6. Characteristic Curves of Surrounding Rock in Xigeda Formation Tunnel

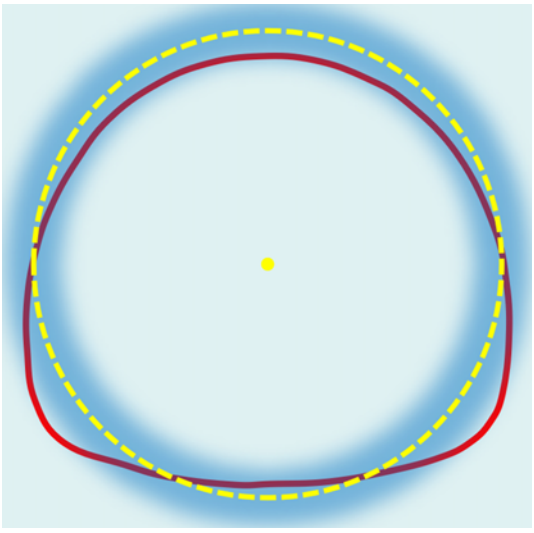

Fig. 7. A Cross-Sectional Similarity Model of Xigeda Formation Tunnel

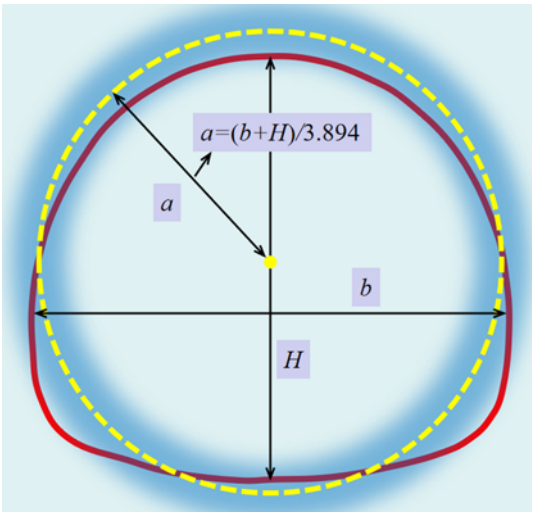

Fig. 8. Similar Circle Solution of Xigeda Formation Tunnel Section

curve. The BC section represents the plastic stage. When the surrounding rock is relatively poor, mudding in water or supporting not timely, plastic zones will appear in the surrounding rock of the tunnel. At the same time, the plastic deformation behavior of the surrounding rock will be prominent, and the deformation around the tunnel will be accelerated on the characteristic curve. The CD section represents the disturbed zone. When the plastic zone of the surrounding rock of the tunnel develops to a certain stage, there will be relaxation within a certain range of the contour around the tunnel. The greatest feature of the disturbed zone is that the surrounding rock pressure belongs to loosening pressure, and at this time the formation pressure acting on the support is the sum of the deformation pressure and the loosening pressure. If support not timely, the surrounding rock will collapse.

The theory of solving the elastoplastic stress and displacement of surrounding rock by circular tunnel section is relatively mature. Since the height-to-span ratio of the Xigeda formation is $H/b = 1157/1296 = 0.893$, the surrounding rock contour is approximated as a circle, as shown in Fig. 7. Therefore, the equivalent circle method can be used to obtain the elastic-plastic stress and displacement of the surrounding rock of the Xigeda formation tunnel.

According to the similar geometric areas and equivalent principle,

$$r = (b+H)/x\,, \tag{6}$$

$$S = \pi r^2\,, \tag{7}$$

where a is the approximate circle radius of the tunnel surrounding rock in the Xigeda formation; x is the relation value between the approximate circle and the actual contour height-to-span parameter; S is the excavation area of the Xigeda formation, taken as 124.67 m^2.

By substituting the construction design value of the Xigeda formation tunnel into the above formula, as shown in Fig. 8, the relationship between the approximate circle radius of the surrounding rock contour of the Xigeda formation tunnel and the actual contour height-to-span parameter is: $a = (b+H)/3.894$.

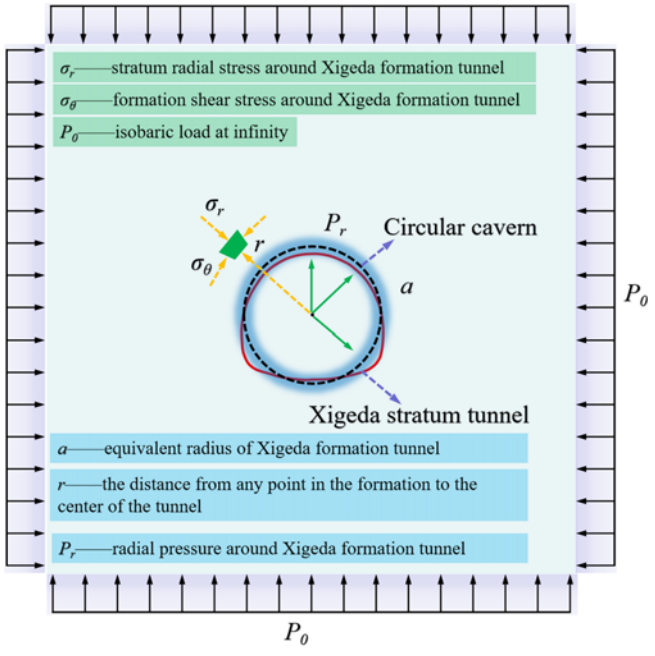

Fig. 9. Mechanical Model of Xigeda Formation Tunnel in Elastic-plastic State

The surrounding rock characteristics curve can be obtained from the elastic-plastic theory of circular tunnel. Fig. 9 shows the elastic-plastic mechanical model of Xigeda formation tunnel. In the model, the irregular tunnel section is replaced by the equivalent circle, which can be calculated by using the circular hole model in the theory of elastic-plastic mechanics to obtain the deformation characteristics of surrounding rock under the redistribution of stratum stress after excavation of Xigeda formation tunnel.

3.1 Solution of Elastic Zone

Under the elastic-plastic state of Xigeda formation tunnel (see Fig. 9), let the tangential stress and radial stress at the elastic-plastic boundary be σ_r^{ep}, σ_θ^{ep}, respectively. The stress and radial displacement at any point in the elastic zone around the tunnel can be determined by elastic theory:

$$\left.\begin{aligned}\sigma_{re} &= P_0 - \left(P_0 - \sigma_r^{ep}\right)\left(R_p/r\right)^2 \\ \sigma_{\theta e} &= P_0 + \left(P_0 - \sigma_r^{ep}\right)\left(R_p/r\right)^2\end{aligned}\right\}, \tag{8}$$

$$u^e = \frac{\left(P_0 - \sigma_r^{ep}\right)R_p^2}{2Gr},\ G = \frac{E}{2(1+\nu)}, \tag{9}$$

where G, E, and ν are the shear modulus, elastic modulus, and Poisson's ratio of surrounding rock respectively. Substituting into the yield criterion Eq. (3), the radial stress at the elastic-plastic boundary can be obtained:

$$\sigma_r^{ep} = \left(2P_0 - B_{ust}\right)/\left(1 + A_{ust}\right). \tag{10}$$

The radial stress at the elastic-plastic boundary can be understood as the minimum support resistance P_{lin} in the elastic zone after excavation.

3.2 Solution of Stress and Plastic Radius in the Plastic Zone

Assuming that the surrounding rock parameters in the plastic zone do not change, the radial stress and tangential stress in the plastic zone are denoted by σ_{rp} and $\sigma_{\theta p}$, and any point in the plastic zone satisfies the static balance Eq. (1) and the yield criterion (3), and solve simultaneous equations can be obtained:

$$\left(A_{ust} - 1\right)\sigma_{rp} + B_{ust} = Cr^{A_{ust}-1}. \tag{11}$$

From the boundary conditions $r=R_0$, $\sigma_{rp} = P_0$, the integral constant C can be determined, and the stress in the plastic zone can be simplified as

$$\left.\begin{aligned}\sigma_{rp} &= \left(P_i + c\cot\varphi\right)\left(r/R_0\right)^{C_{ust}} - c\cot\varphi \\ \sigma_{\theta p} &= A_{ust}\left(P_i + c\cot\varphi\right)\left(r/R_0\right)^{C_{ust}} - c\cot\varphi\end{aligned}\right\}, \tag{12}$$

where $C_{ust} = \left[4(1+b)\sin\varphi\right]/\left[(2+b)(1-\sin\varphi)\right]$. The radial stress at the elastic-plastic boundary not only satisfies the elastic condition but also satisfies the stress formula of the plastic zone. Therefore, combining Eq. (8), the plastic zone radius can be obtained:

$$R_p = R_0\left(\frac{\sigma_r^{ep} + c\cot\varphi}{P_i + c\cot\varphi}\right)^{1/C_{ust}}. \tag{13}$$

3.3 Solution of Radial Displacement of Surrounding Rock under Elastic-Plastic State

A plastic zone with a radius R_p is formed in a certain range around the tunnel. The strain of the surrounding rock in the plastic zone consists of elastic strain and plastic strain, that is, $\varepsilon_r = \varepsilon_r^e + \varepsilon_r^p$, $\varepsilon_\theta = \varepsilon_\theta^e + \varepsilon_\theta^p$. The surrounding rock in the plastic zone obeys the generalized Hook law, namely

$$\left.\begin{aligned}\varepsilon_r^e &= (1+\nu)\left[(1-\nu)\left(\sigma_r - P_0\right) - \nu\left(\sigma_\theta - P_0\right)\right]/E \\ \varepsilon_\theta^e &= (1+\nu)\left[(1-\nu)\left(\sigma_\theta - P_0\right) - \nu\left(\sigma_r - P_0\right)\right]/E\end{aligned}\right\}. \tag{14}$$

From Eq. (4), the following is obtained:

$$\varepsilon_r + \beta\varepsilon_\theta = \varepsilon_r^e + \beta\varepsilon_\theta^e + \varepsilon_r^p + \beta\varepsilon_\theta^p = \varepsilon_r^e + \beta\varepsilon_\theta^e. \tag{15}$$

By substituting Eq. (2) into Eq. (15), the following is obtained:

$$\varepsilon_r + \beta\varepsilon_\theta = \frac{du}{dr} + \beta\frac{u}{r} = \varepsilon_r^e + \beta\varepsilon_\theta^e. \tag{16}$$

Solve the differential equation and consider the radial displacement $u = u^{ep}$ at the elastic-plastic boundary $r = R_p$ to obtain:

$$u = r^{-\beta}\int_{R_p}^{r} r^\beta\left(\varepsilon_r^e + \beta\varepsilon_\theta^e\right)dr + u^{ep}\left(R_p/r\right)^\beta, \tag{17}$$

$$u^{ep} = \left(P_0 - \sigma_r^{ep}\right)R_p/(2G). \tag{18}$$

Combine Eq. (14) and Eq. (17) to obtain the displacement solution of the surrounding rock plastic zone (Zhang and Zeng, 2015):

$$\left.\begin{aligned}u &= \frac{1}{2G}r^{-\beta}\left[C_1 r^{\beta+1}\left(P_i + c\cot\varphi\right) + C_2 r^{\beta+1} + C_3 R_p^{\beta+1}\right] \\ C_1 &= \left[1 - \left(1 + A_{ust}\right)\nu + \beta\left(A_{ust} - A_{ust}\nu - \nu\right)\right]/\left(\beta + C_{ust} + 1\right) \\ C_2 &= \left(2\nu - 1\right)\left[P_0 + c\cot\varphi\right] \\ C_3 &= P_0 - \sigma_r^{ep} - C_1\left(\sigma_r^{ep} + c\cot\varphi\right) - C_2\end{aligned}\right\}. \tag{19}$$

The above formula is a unified solution for the displacement of the circular tunnel surrounding rock considering the dilatancy of the plastic zone and the real elastic strain. When $r = R_0$, Eq. (19) reflects the relationship between the radial displacement at the inner wall of the tunnel and the support reaction. The dilatancy angle ψ of the plastic zone of the surrounding rock can be obtained by conventional geotechnical tests or by empirical methods.

3.4 Solution of Radial Displacement of Surrounding Rock in the Disturbed Zone

As the plastic zone of the surrounding rock develops, the stratum surrounding the tunnel will produce loose pressure on the lining, so the formation pressure acting on the lining under the third stress state ought to be the sum of the deformation pressure and the loosening pressure. As shown in Fig. 6, the pressure in the disturbed zone shows a rebound uptrend.

For circular tunnels under hydrostatic pressure, assuming that the stratum disturbed zone is the concentric circle of the tunnel and the body force is distributed along the radial direction, the loosening pressure can be obtained by the static equilibrium condition of the unit body on the vertical axis:

$$P_0 = -c\cot\varphi + \cot\varphi\left(\frac{r}{R_p}\right)^{\beta-1} + \frac{\gamma r}{\beta-2}\left[1-\left(\frac{r}{R_p}\right)^{\beta-2}\right]. \quad (20)$$

From Eq. (12), the displacement solution of the disturbed zone around the tunnel under the action of the uniform load P_0 is

$$u = -\frac{1}{2G}P_0\left(\frac{R_p}{r}\right)^{\beta+1} r\,. \quad (21)$$

4. Decoupling Analysis of Interaction between Surrounding Rock and Support

4.1 The Analytical Process of the Whole Process of Interaction between Surrounding Rock and Support

Based on the unified solution of the radial displacement of the circular tunnel, considering the hardening properties of shotcrete, this paper analyzes the interaction process between the tunnel surrounding rock and the support. The specific implementation steps are as follows:

1. Based on the unified strength theory, considering the influence of the intermediate principal stress and dilatancy on the deformation of the tunnel surrounding rock, use the calculation of radius for equivalent circle to convert the non-circular tunnel section into a circular tunnel section with an equivalent radius, and establish the corresponding convergence curve of the surrounding rock of the circular tunnel so that the deformation of surrounding rock is a function of supporting force as $u=f_{ust}(P_i)$;
2. Select a reasonable prediction formula for the longitudinal deformation of the tunnel, such as the displacement release coefficient formula based on the maximum plastic radius, as shown in Eq. (5);
3. Assuming that the support is erected at a distance of L_0 from the tunnel face, and this position is taken as the selected section, the initial radial displacement u_{ini} of the surrounding rock during support is obtained from the displacement release coefficient formula;
4. Taking time t as the basic variable, and taking the time when the support structure is just constructed as zero time, let the tunnel is advancing at the excavation speed V and the time increment as Δt, so at the time t_n, the distance between the tunnel face and the selected section is $L_n = V\cdot t_n + L_0$;
5. At a position L_n far away from the tunnel face, calculate the radial displacement u_{fn} without support according to the displacement release coefficient formula (5), and obtain the virtual support pressure of the tunnel face $P_{f,n}=f_{ust}^{-1}(u_{f,n})$ by coupling the longitudinal deformation profile and the ground reaction curve;
6. Determine the support stiffness of the primary support at time t_n. The integral support stiffness of the shotcrete and steel frame combination is calculated as follows:

$$K_{tot}(t_n) = k_{shot}(t_n) + k_{set}\,. \quad (22)$$

At time t_n, the support force of surrounding rock can be regarded as the virtual support pressure $P_{f,n}$ generated by the spatial effect of the tunnel face and the support resistance $P_{s,n}$ of the actual support structure. After the support structure is applied, the deformation increment of surrounding rock is consistent with the support deformation, so the radial displacement value of surrounding rock can be obtaine:

$$\begin{aligned} u_{tot,n} &= f_{ust}\left(P_n = P_{f,n} + P_{s,n}\right) \\ &= f_{ust}\left(P_n = P_{f,n} + k_{tot}(t_n)\cdot\left(u_{tot,n} - u_{ini}\right)\right). \end{aligned} \quad (23)$$

Repeat steps (4) – (7), the virtual support pressure decreases gradually, and the support resistance increases continuously. Finally, when the virtual support pressure can be ignored, the surrounding rock and the support reach an equilibrium state, and the support resistance in the equilibrium state is P_{eq}.

4.2 Mechanical Characteristics of Primary Support

The strength of shotcrete depends on the hydration degree. With the progress of hydration, its strength and elastic modulus will increase, and finally stabilize. In the early stage of support, the insufficient strength of shotcrete increases the possibility of structural failure. Therefore, the hardening properties of shotcrete should be considered when analyzing the mechanical capability of tunnel support. Use the equation proposed by Weber and Potter to describe the hardening law of shotcrete (Einstein and Schwartz, 1979)

$$\left.\begin{aligned} \sigma_{shot}(t) &= \sigma_0\left(1-e^{-\beta t}\right) \\ E_{shot}(t) &= E_0\left(1-e^{-\alpha t}\right) \end{aligned}\right\}, \quad (24)$$

where σ_0 and E_0 are the final compressive strength and elastic modulus of shotcrete respectively, α and β are the hardening time constants, usually $\alpha=\beta$.

It is not necessary to consider the mesh reinforcement when calculating the support stiffness of shotcrete, but when adding section steel frame and grid steel frame to the shotcrete, it is necessary to consider the superimposition effect of the two types of support at the same time. The stiffness of the primary support can be solved according to the thick-walled cylinder problem of the elastic theory

$$k_{shot(set)}(t_n) = \frac{E_{shot(set)}(t_n)\left[R^2 - \left(R - t_{shot(set)}\right)^2\right]}{\left(1+\nu_{shot(set)}\right)R\left[\left(R-t_{shot(set)}\right)^2 + \left(1-2\nu_{shot(set)}\right)R^2\right]}, \quad (25)$$

where R is the outer diameter of the cylinder, $k_{shot(set)}$, $E_{shot(set)}$, $\nu_{shot(set)}$, and $t_{shot(set)}$ are the supporting stiffness of the shotcrete or steel frame, elastic modulus, Poisson's ratio and equivalent thickness, respectively, and the parameters of the shotcrete are related to time.

4.3 Analysis of Interaction between Surrounding Rock and Support

During the elastic-plastic analysis of the surrounding rock, the

surrounding rock may only produce elastic deformation, or it may produce both elastic deformation and plastic deformation. Therefore, there are two different situations in step (7) of the analysis process of the interaction between the surrounding rock and the support. Whether the surrounding rock produces plastic deformation during the primary support can be judged by the critical support force, that is, comparing the virtual support pressure $P_{f,ini}$ and P_{lin} of the tunnel face at the support position, so it is divided into the following two categories:

1. The surrounding rock only produces elastic deformation during support, that is, $P_{f,ini} \geq P_{lin}$.
   The distance between the selected section and the tunnel face is L_n, and the inner wall of the tunnel produces elastic deformation $u^e_{tot,n}$ under the combined action of the virtual support pressure $P_{f,n}$ and the support reaction $P_{s,n}$ provided by the primary support. It expresses

$$u^e_{tot,n} = (1+\nu)\left(P_0 - P_{f,n} - P_{s,n}\right)R_0 / E. \tag{26}$$

   At this time, the radial displacement at the outer diameter of the primary support is $u^e_{R_0,n}$, and the support resistance $P_{s,n}$ is

$$P_{s,n} = K_{tot}(t_n)\cdot u^e_{R_0,n} = K_{tot}(t_n)\cdot\left(u^e_{tot,n} - u_{ini}\right), \tag{27}$$

   where $u_{ini} = u_{\max}\left\{1-\left[1-\frac{1}{3}\exp\left(-0.15R^*\right)\right]\exp\left(-1.5L_0 / R_p^{\max}\right)\right\}$,

   $u_{\max}$ is the maximum radial displacement of the inner wall of the tunnel without support; $u^e_{R_0,n}$ should not be greater than the maximum elastic displacement $u^s_{\max}$ of the support structure, and $u^e_{R_0,n}$ can be obtained from the maximum support force and the support stiffness.
   Correspondingly, the virtual support pressure $P_{f,n}$ at a distance of L_n from the tunnel face can be obtained by the following formula:

$$P_{f,n} = P_0 - 2G\cdot u^e_{f,n} / R_0, \tag{28}$$

   where $u^e_{f,n} = u_{\max}\left\{1-\left[1-\frac{1}{3}\exp\left(-0.15R^*\right)\right]\exp\left(-1.5L_n / R_p^{\max}\right)\right\}$.

   Substituting Eq. (28) and Eq. (27) into Eq. (26), respectively, the analytical solution of surrounding rock deformation when supporting in the elastic stage is obtained:

$$u^e_{tot,n} = \frac{P_0 - P_{f,n} + K_{tot}(t_n)\cdot u_{ini}}{2G / R_0 + K_{tot}(t_n)}. \tag{29}$$

   L_n should be within the influence range of the spatial effect of the tunnel face, and L_n can be determined by the advancing speed: $L_n = V\cdot t_n$.
2. The surrounding rock produces elastic-plastic deformation during support, that is, $P_{f,ini} \leq P_{lin}$.
   For the selected section whose distance to the tunnel face is

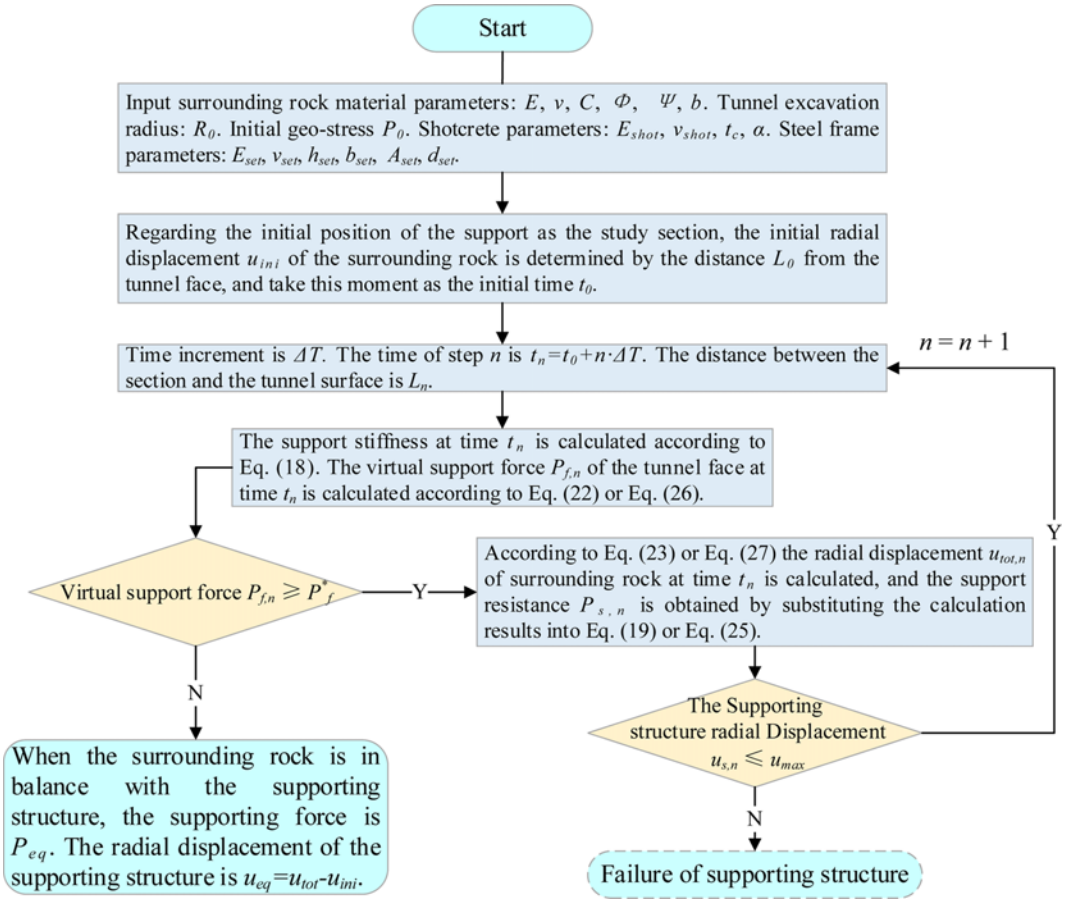

Fig. 10. Solving Procedure

L_n, the tunnel produces elastic-plastic deformation $u^p_{tot,n}$ under the combined action of the virtual support pressure $P_{f,n}$ and the support resistance $P_{s,n}$, then the displacement calculation formula for the inner wall of the tunnel at this moment is expressed:

$$u^p_{tot,n}=\frac{1}{2G}R_0^{-\beta}\begin{bmatrix}C_1R_0^{\beta+1}\left(P_{f,n}+P_{s,n}+c\cot\varphi\right)\\+C_2R_0^{\beta+1}+C_3R_p^{\beta+1}\end{bmatrix}. \tag{30}$$

When the radial displacement at the outer diameter of the primary support is $u^e_{R_0,n}$, the support resistance $P_{s,n}$ can be obtained:

$$P_{s,n}=K_{tot}\left(t_n\right)\cdot u^e_{R_0,n}=K_{tot}\left(t_n\right)\cdot\left(u^p_{tot,n}-u_{ini}\right). \tag{31}$$

Correspondingly, the virtual support pressure $P_{f,n}$ at a distance of L_n from the tunnel face L_n can be solved by the following formula:

$$u^p_{f,n}=\frac{1}{2G}R_0^{-\beta}\begin{bmatrix}C_1R_0^{\beta+1}\left(P_{f,n}+c\cot\varphi\right)\\+C_2R_0^{\beta+1}+C_3R_p^{\beta+1}\end{bmatrix}. \tag{32}$$

Eq. (32) is a transcendental equation, which cannot give an analytical solution, but the numerical solution of $P_{f,n}$ can be obtained through numerical analysis methods.

Substituting the calculated virtual support pressure and support resistance into Eq. (32), the analytical equation of surrounding rock deformation when supporting in the plastic stage is obtained:

$$u^p_{tot,n}=\frac{1}{2G}R_0^{-\beta}\begin{Bmatrix}C_1R_0^{\beta+1}\left[P_{f,n}+K_{tot}\left(t_n\right)\cdot\left(u^p_{tot,n}-u_{ini}\right)\right]\\+C_1R_0^{\beta+1}\cdot c\cot\varphi+C_2R_0^{\beta+1}+C_3R_p^{\beta+1}\end{Bmatrix}. \tag{33}$$

Equation (33) is also a transcendental equation, and the surrounding rock displacement can also be solved by numerical analysis.

The above analysis process of the interaction between surrounding rock and support of the tunnel is realized by MATLAB programming, and the solution process is shown in Fig. 10.

5. Analysis of the Whole Process of Interaction between Surrounding Rock and Support of Tunnel in Xigeda Formation

Taking the shale sandstone in the Xigeda formation of the new Chengdu-Kunming Railway expansion and reconstruction project as the research object, analyze the whole process of the interaction between the surrounding rock and the support of the tunnel, and focus on the influence law of various factors on the analysis results. Physical and mechanical parameters of the formation are selected as shown in Table 1.

5.1 The Influence of the Unified Strength Theoretical Parameter *B*

When the intermediate principal stress effect in the rock mass is different, the range of plastic zone and stress distribution of the tunnel surrounding rock will be different respectively, which results in different displacement release rates at the same position,

Table 1. Physical and Mechanical Parameters of Shale Sandstone Xigeda Formation Strata

Water content%	Unit weight (kN/m^3)	Elastic modulus (E/MPa)	Poisson's ratio	Cohesion (kPa)	Internal friction angle (°)	Dilatancy angle (°)
0%	19.5	323.15	0.4	343.4	44.5	5.6
5%	19.5	315.90	0.4	322.8	40.7	5.1
10%	19.5	308.00	0.4	302.1	36.8	4.6
15%	19.5	300.10	0.4	281.4	33.0	4.1
20%	19.5	292.25	0.4	260.7	29.1	3.6
25%	19.5	203.00	0.4	196.3	24.8	3.1
26.6%	19.5	150.60	0.4	155.2	24.1	3.0

Note: 26.6% is natural moisture content.

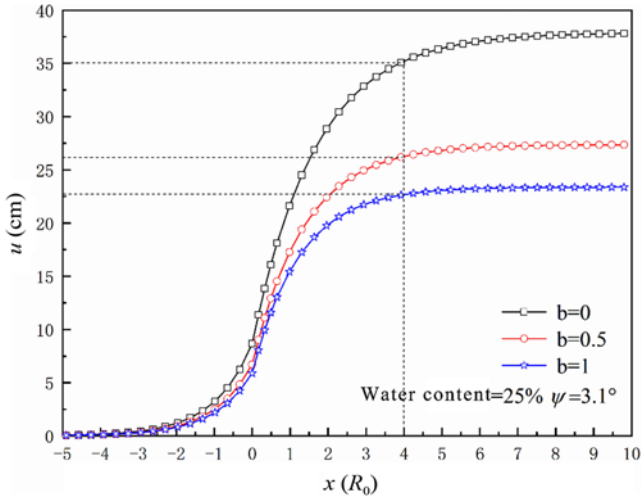

Fig. 11. Influence of Unified Strength Theory Parameter b on Tunnel LDP Curve

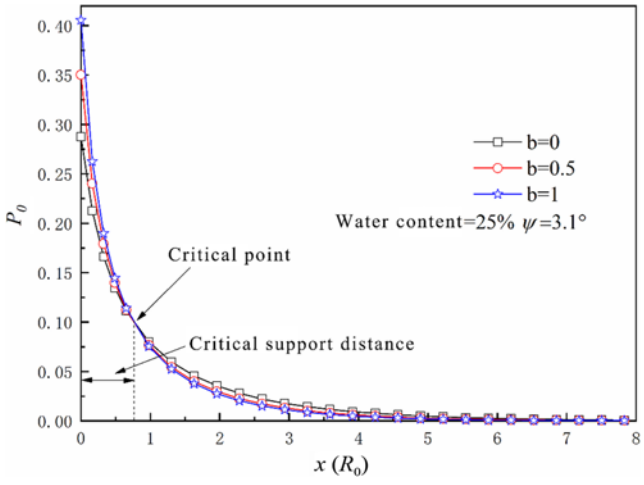

Fig. 12. Influence of Unified Strength Theory Parameter b on Virtual Support Pressur

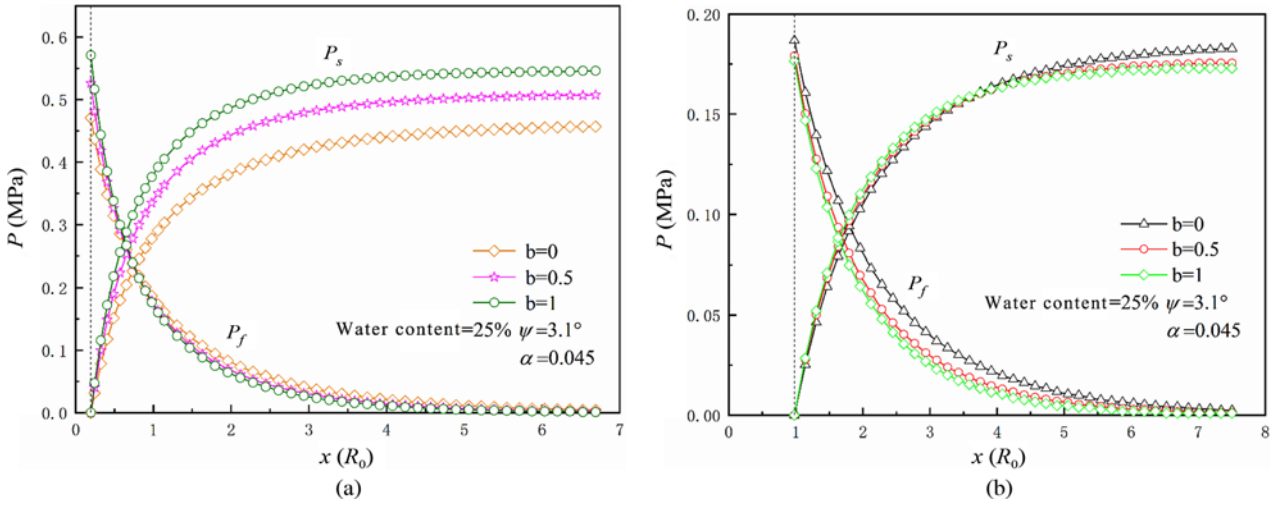

Fig. 13. Influence of Unified Strength Theory Parameter b on Distribution Curve of Virtual Support Pressure and Support Counter-Force: (a) Support before Critical Point, (b) Support after Critical Point

affecting the size of the virtual support pressure in turn. Taking 25% water content of the surrounding rock as an example, analyze the influence of the unified strength theoretical parameter b on the tunnel LDP curve and virtual support pressure, the results are shown in Fig. 11 and Fig. 12 respectively.

Analyze from Fig. 11, it can be obtained:

1. The influence of the intermediate principal stress on the LDP curve is very significant. The smaller the intermediate principal stress effect of the surrounding rock is, the larger the plastic radius of the surrounding rock and the radial displacement of the inner wall of the tunnel will be, and the LDP curve uplifts overall.
2. At twice the tunnel diameter from tunnel face, when b is 0, 0.5, and 1, the displacement release rate is 75.24%, 81.96%, and 84.54% respectively, that is, the displacement release rate will increase with the increase of b.
3. When b = 1, the influence range of the tunnel face spatial effect is about 2.5 times the excavation diameter. When b = 0, the tunnel face spatial effect disappears after about 4 times the tunnel diameter. The greater the intermediate principal stress effect of the rock, the more forward the position where the tunnel displacement tends to be stable, and the smaller the influence range of the spatial effect of the tunnel face.

According to Fig. 12, the virtual support pressure distribution curves with different b values have intersection points at 0.8 times the tunnel radius. These intersection points are called the critical point of support, and the distance between the critical point and the tunnel face is called the critical distance. Before the critical point, the virtual support pressure increases with the increase of parameter b. After the critical point, the larger b is, the smaller the virtual support pressure is. Analysis of the reasons shows that for a certain section before the critical point of the support, although the displacement release rate will decrease with the decrease of b, the maximum tunnel wall displacement will increase accordingly. When the maximum tunnel wall displacement has a stronger influence, the cave wall displacement will be greater, and the corresponding virtual support pressure will be smaller. When the distance from the tunnel face is far, the stress release of surrounding rock with stronger intermediate principal stress effect has been basically completed, so the corresponding virtual support pressure is smaller.

When erecting the support, the value of the virtual support pressure directly affects the force of the support structure. The development curves of the supporting reaction when the steel composite support structure is erected before and after the critical point are shown in Fig. 13 respectively.

Figure 13 reflects the segmentation of the influence of the intermediate principal stress effect on the support force. The final force state of the support structure is positively correlated with the virtual support pressure when the support is erected. When the support is erected before the critical point, the stronger the intermediate principal stress effect of the surrounding rock, the greater the virtual support pressure, and the greater the support force of the support structure. On the contrary, when the support is erected after the critical point, the virtual support pressure and the ultimate support reaction of the support structure increase with the weakening of the intermediate principal stress effect of the surrounding rock. Therefore, when designing the support structure, truthfully considering the intermediate principal stress effect of the surrounding rock can fully utilize the self-bearing capacity of the surrounding rock, and can also guide the support design more effectively.

5.2 The Influence of Dilatancy Angle

The dilatancy of surrounding rock mainly affect the deformation of the plastic zone, especially at the inner wall of the tunnel. The dilatancy of surrounding rock do not affect the plastic radius, so in the same location of the tunnel, different dilatancy angles do

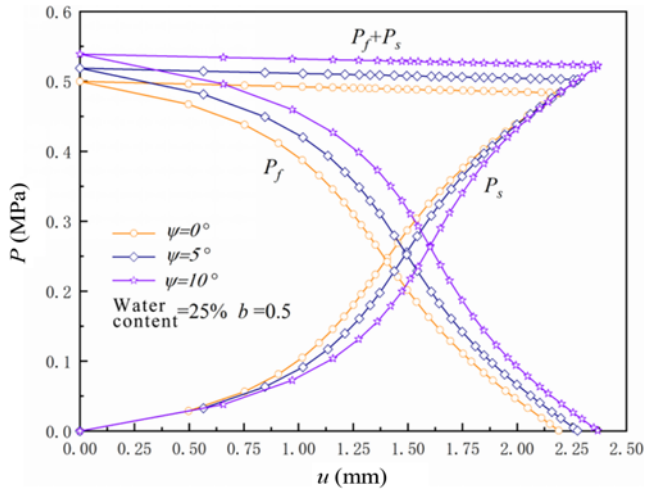

Fig. 14. Influence of Dilatancy Angle on Development Curve of Virtual Support Pressure and Support Counter-Force

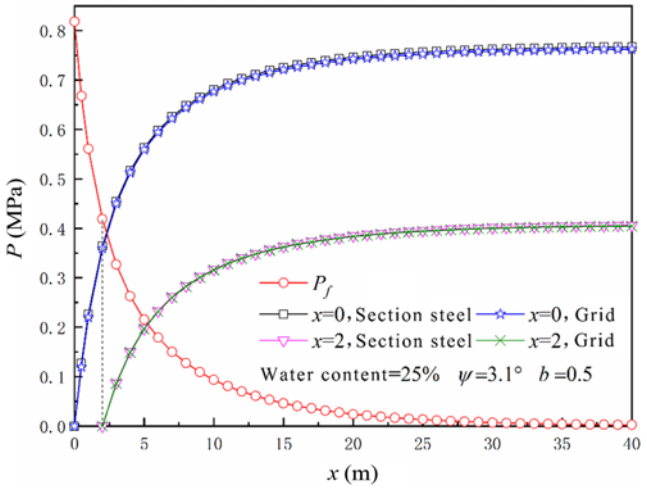

Fig. 15. Influence of Stiffness on Distribution Curve of Virtual Support Pressure and Support Counter-Force

not change the displacement release coefficient. During the tunnel excavation, excessive deformation of the surrounding rock is not allowed, but the tunnel deformation will increase with the increase of the dilatancy angle, and the impact is very significant. Therefore, it is necessary to analyze the influence of the dilatancy angle on the interaction between surrounding rock and support from the perspective of deformation control. Taking the relative deformation value u / R_0=1.58% of surrounding rock as the starting point of support, the influence of different dilatancy angles on the development curve of virtual support pressure and support reaction is shown in Fig. 14.

It can be seen from Fig. 14 that when the dilatancy angle is 0°, 5° and 10°, the final reaction of the support structure is 0.483 MPa, 0.502 MPa and 0.522 MPa respectively. Therefore, the greater the dilatancy angle is, the greater the virtual support pressure during the erection of the support structure is, and the greater the supporting force of the final support structure is. On the one hand, the design of the support structure considering the dilatancy of the surrounding rock can accurately predict the degree of deformation of the surrounding rock, on the other hand, it also makes the surplus safety performance of the support structure more abundant.

5.3 The Influence of Support Stiffness

At present, the primary support steel arch of the tunnel mainly uses the grid steel frame and the section steel frame. Due to the difference of the support stiffness, the control effect and the application scope of the two on the surrounding rock deformation are different. The support reaction and virtual support pressure distribution curves of different combined support structures and the deformation distribution curves of the support structure are respectively shown in Figs. 15 and 16.

According to Figs. 15 and 16, the final force of the primary support of different steel arch types will also be different. Since the support stiffness of the section steel frame is greater, the

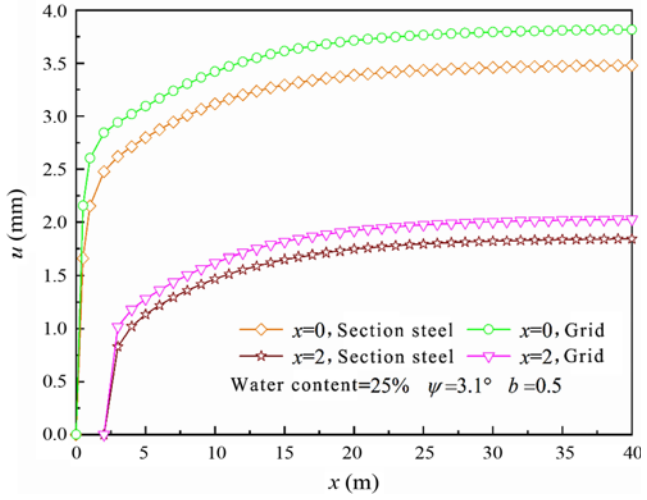

Fig. 16. Influence of Stiffness on Deformation Distribution Curve of Support Structure

support reaction will also be greater. When supporting immediately after excavation, the ultimate support force provided by the combined support structure of section steel frame is only 0.6% greater than that of the combined support structure of grid steel frame. When the support structure is erected at a distance of 2 m from the tunnel face, the gap between the two is even smaller. At the same time, the two types of support will also differ in the control of surrounding rock deformation. The deformation of the combined support structure of section steel frame is smaller than that of the grid. When supporting immediately after excavation, the former is 9.7% smaller than the latter. When the support is erected at a distance of 2 m from the tunnel face, the former is 10.2% smaller than the latter.

5.4 The Influence of Supporting Opportunity

In fact, the final force of the support structure is mainly related to the virtual support pressure at the primary support position, that is, the influence of supporting opportunity is very severe. The

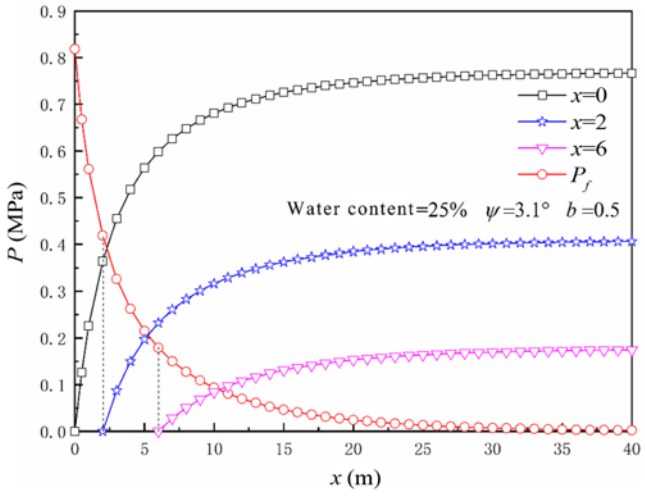

Fig. 17. Influence of Supporting Time on Distribution Curve of Virtual Support Pressure and Support Counter-Force

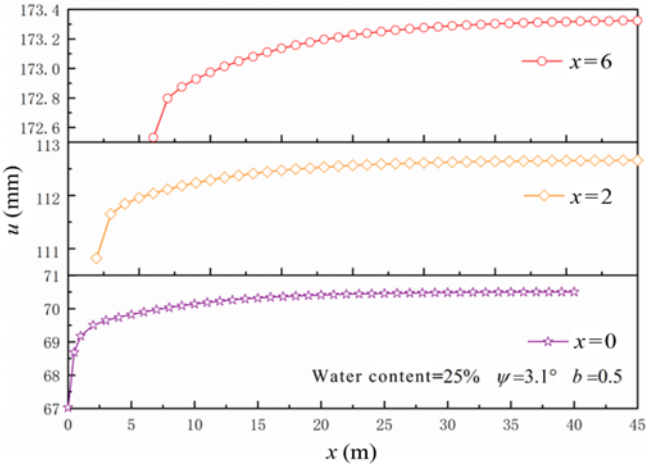

Fig. 18. Influence of Supporting Time on Deformation Distribution Curve of Support Structure

support reaction distribution curve and the support structure deformation curve of the combined support structure of section steel frame under different supporting times are shown in Figs. 17 and 18.

From Figs. 17 and 18, it can be seen that the primary support position has a significant impact on the force and deformation of the support system. Immediately supporting after excavation, the support force provided by the final support system is 1.9 and 4.4 times that of $x = 2m$ and $x = 6m$, respectively. Although premature support will make the support system bear greater load, the control effect on surrounding rock deformation will be better. When the primary support distance is $x = 2m$ and $x = 6m$, the final deformation of surrounding rock is 1.60 times and 2.46 times, respectively. It can be seen that the closer the primary support position is, the smaller the deformation of the surrounding rock and the greater the force on the support structure will be.

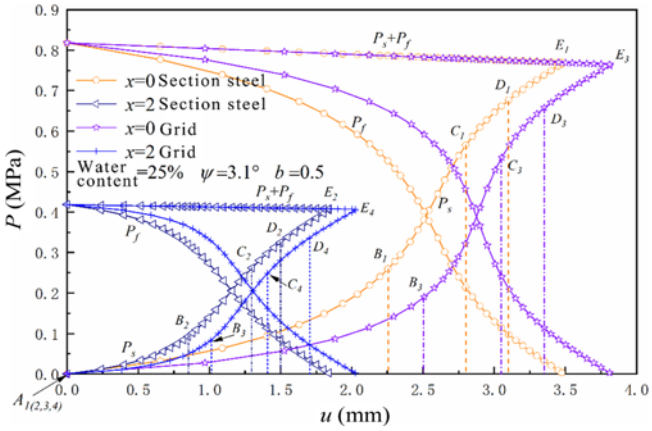

Fig. 19. The Complete Process Curve of Virtual Support Pressure and Support Counter-Force

5.5 Influence of Hardening Properties

Due to the hardening properties of shotcrete, the primary support stiffness of the tunnel does not increase linearly. Fig. 19 shows the whole development process curve of the virtual support pressure provided by the spatial effect of the tunnel face and support reaction of the section support.

Figure 19 shows the whole process of the change of the support reaction P_s and the virtual support pressure P_f, in which the force and deformation of the support structure shows obvious stages. In the initial stage of support construction, the stiffness of the combined support system is low. Under the action of lower supporting force, greater deformation will occur, and the support reaction curve will be relatively flat, that is the slow growth stage (*AB*). As the shotcrete continues to harden, the supporting stiffness will increase rapidly in the short term. The virtual support pressure also decreases rapidly, and the supporting force of the support structure also increases rapidly, that is the accelerated growth stage (*BC*). As time flows, the stiffness growth rate of the support composite system slows down, the spatial constraint effect of the tunnel face weakens, and the growth rate of the support force slows down accordingly, that is the slowing growth stage (*CD*). When the strength of the shotcrete gradually stabilizes, the stiffness of the support composite system also remains the same, then the structural deformation and the support force are in a linear relationship, that is the final stabilization stage (*CE*). Finally, support structure bears all the surrounding rock pressure, and the surrounding rock and the support reach a equilibrium state, that is the point *E* in Fig. 19.

Both the hardening parameters of shotcrete and the stiffness of the steel arch affect the force and deformation of the support structure. In order to fully study the degree of influence, the deformation distribution curves of the support structure under different hardening parameters are drawn, as shown in Fig. 20.

The steel arch can provide support force immediately after erection. Therefore, in the initial stage of support where the shotcrete cannot meet the strength requirements, the steel arch can bear the pressure of the surrounding rock and control the

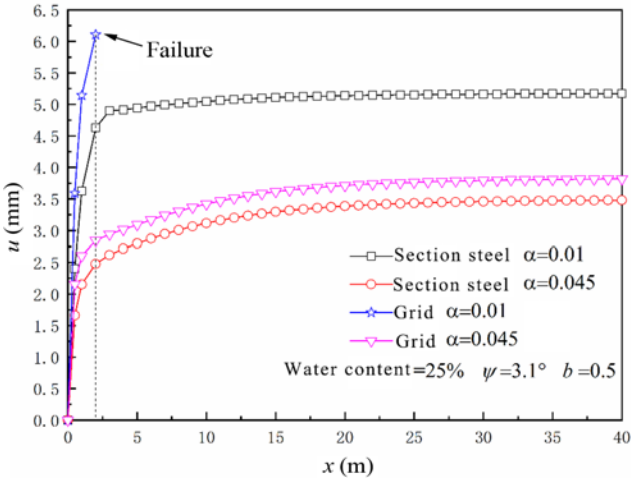

Fig. 20. Influence of Hardening Parameter on Deformation Distribution Curve of Support Structure

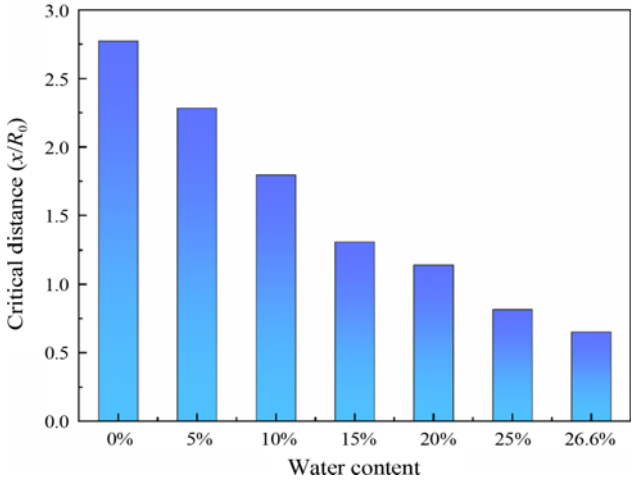

Fig. 21. Influence of Moisture Content on Critical Support Distance

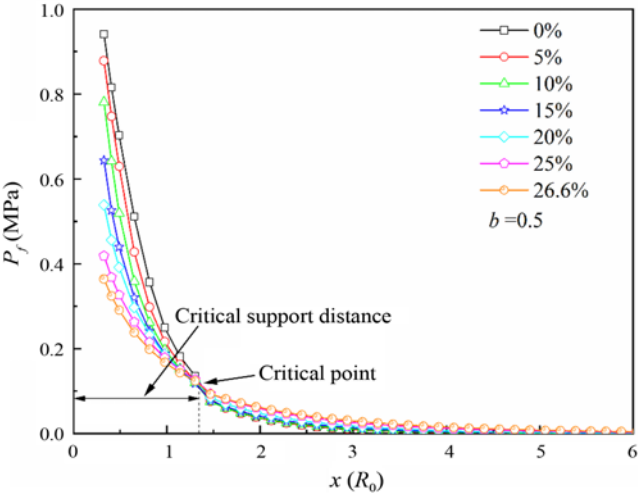

Fig. 22. Influence of Moisture Content on Virtual Support Pressure

deformation of the surrounding rock. If the shotcrete hardening rate is too slow or the excavation speed is too fast, the stress release speed will be too fast, the early strength of the support structure will be insufficient, and structural failure and damage are prone to occur. Among them, the combined support structure of grid steel frame is more sensitive to hardening parameters and excavation speed due to lower stiffness. According to Fig. 20, for the combined support structure of section steel frame, when the hardening parameter is 0.01, the final deformation is increased by 48.6% compared with the hardening parameter of 0.045. When using the grid and shotcrete combination system, the support structure fails to meet the safety requirements when the hardening parameter is 0.01.

5.6 Influence of Water Content

The most notable feature of the Xigeda formation is mudding in water, and its engineering mechanical properties are quite different under different water content. Therefore, it is necessary to explore the influence of water content on the interaction between surrounding rock and support. In the above analysis of the influence of the unified strength theoretical parameter b on the virtual support pressure, it is pointed out that there is a critical support point and the critical support distance. The critical distance under different surrounding rock water content is calculated, as shown in Fig. 21. When the water content of surrounding rock increases, the critical position of support is closer to the tunnel face. When the water content is 0%, the critical distance is 2.77 times the tunnel radius. When the water content increases to 26.6%, the critical distance decreases to 0.65 times the tunnel radius, which decreases by 76.8%. In fact, this is related to the quality of the surrounding rock. The higher the water content is, the worse the quality of the surrounding rock is, the slower the stress release process is, and the intersection of the corresponding virtual support pressure change curve will move forward.

Not only does the influence of the intermediate principal stress on the virtual support pressure have a critical support point, but the influence of the water content also shows a similar law. Fig. 22 is the distribution curve of the virtual support pressure under different water content. According to the Fig. 22, before the critical support point, the virtual support pressure decreases with the increase of water content; after the critical support point, the virtual support pressure increases with the increase of water content, which means that when the support structure is erected before or after the critical point, the water content has a different influence on the virtual support pressure.

6. Conclusions

Based on the formation characteristics of the Xigeda formation, this paper proposes a solution method to analyze the interaction process between the surrounding rock and support of the tunnel. Through decoupling analysis of dependent variables, the following conclusions are obtained:

1. There will be intersection points in the virtual support pressure variation curves of different parameters b, which is called the critical support point. Before the critical point,

due to the influence of the maximum displacement of the tunnel wall, the virtual support pressure will increase with the increase of the intermediate principal stress effect. After the critical point, when the intermediate principal stress effect of the surrounding rock is weak, the stress release process is slower, so the virtual support pressure at the same position will be greater.

2. When analyzing the influence of dilatancy from the perspective of deformation control, the ultimate load of the support structure will increase with the increase of the dilatancy angle. Therefore, the dilatancy of the surrounding rock should be considered reasonably when designing the support structure.
3. When considering the hardening properties of shotcrete, the whole process of force and deformation of the combined support structure of steel frame can be divided into four stages: slow growth stage (*AB*), accelerated growth stage (*BC*), and slow growth stage (*CD*) and the stabilization stage (*CE*), which are determined by the shotcrete hardening parameters and the virtual support pressure variation law.
4. The combined support structure of section steel frame and grid steel frame has the same effect on the deformation control of the surrounding rock, and the force of the support structure is also relatively small. Due to lower supporting stiffness of grille steel frame, it is more sensitive to hardening parameters.
5. When the unified strength theoretical parameter b is constant, the higher the water content, the worse the quality of the surrounding rock, the slower the stress release process, and the lower critical distance of support. At the same time, there is also a critical point in the influence of water content on virtual support pressure, and the change law of virtual support pressure is opposite before and after the critical point.

Acknowledgements

The research work herein was supported by National Natural Science Foundation of China (Grant No.51678498) and the High Speed Railway and Natural Science United Foundation of China (U1934213).

ORCID

Ping Zhou https://orcid.org/0000-0003-0122-034X
Feicong Zhou https://orcid.org/0000-0002-4053-9508
Jiayong Lin https://orcid.org/0000-0001-5243-1935
Jinyi Li https://orcid.org/0000-0003-3586-4629
Yifan Jiang https://orcid.org/0000-0002-8736-3466
Bao Yang https://orcid.org/0000-0002-2496-5072
Zhijie Wang https://orcid.org/0000-0001-9559-3512

References

Alejano LR, Rodriguez-Dono A, Veiga M (2012) Plastic radii and longitudinal deformation profiles of tunnels excavated in strain-softening rock masses. *Tunnelling and Space Technology* 30:169-182, DOI: 10.1016/j.tust.2012.02.017

Carranza-Torres C, Fairhurst C (2000) Application of the convergence-confinement method of tunnel design to rock masses that satisfy the Hoek-Brown failure criterion. *Tunnelling and Underground Space Technology* 15(2):187-213, DOI: 10.1016/S0886-7798(00)00046-8

Carranza-Torres C, Rysdahl B, Kasim M (2013) On the elastic analysis of a circular lined tunnel considering the delayed installation of the support. *International Journal of Rock Mechanics and Mining Sciences* 61:57-85, DOI: 10.1016/j.ijrmms.2013.01.010

Cui L, Zheng JJ, Zhang RJ, Lai HJ (2015) A numerical procedure for the fictitious support pressure in the application of the convergence-confinement method for circular tunnel design. *International Journal of Rock Mechanics and Mining Sciences* 78:336-349, DOI: 10.1016/j.ijrmms.2015.07.001

Cui L, Zheng JJ, Zhang RJ, Zhang W (2014) Elastoplastic solutions to strain-softening behavior of surrounding rock masses of deep circular tunnels considering dilatancy effect. *Rock and Soil Mechanics* 35(4):1187-1193 (in Chinese)

Einstein HH, Schwartz CW (1979) Simplified analysis for tunnel supports. *Journal of the Geotechnical Engineering Division* 105(4):499-518, DOI: 10.1061/AJGEB6.0000786

Es-Haghi MS, Shishegaran A, Rabczuk T (2020) Evaluation of a novel asymmetric genetic algorithm to optimize the structural design of 3D regular and irregular steel frames. *Frontiers of Structural and Civil Engineering* 14(5):1110-1130, DOI: 10.1007/s11709-020-0643-2

Fahimifar A, Ranjbarnia M (2009) Analytical approach for the design of active grouted rockbolts in tunnel stability based on convergence-confinement method. *Tunnelling and Underground Space Technology* 24(4):363-375, DOI: 10.1016/j.tust.2008.10.005

Gschwandtner GG, Galler R (2012) Input to the application of the convergence confinement method with time-dependent material behaviour of the support. *Tunnelling and Underground Space Technology* 27(1):13-22, DOI: 10.1016/j.tust.2011.06.003

Jin YF, Zhu BQ, Yin ZY, Zhang DM (2019) Three-dimensional numerical analysis of the interaction of two crossing tunnels in soft clay. *Underground Space* 4(4):310-327, DOI: 10.1016/j.undsp.2019.04.002

Khalid MS, Kikumoto M, Cui Y, Kishida K (2019) The role of dilatancy in shallow overburden tunneling. *Underground Space* 4(3):181-200, DOI: 10.1016/j.undsp.2018.09.006

Kwong AKL, Ng CCW, Schwob A (2019) Control of settlement and volume loss induced by tunneling under recently reclaimed land. *Underground Space* 4(4):289-301, DOI: 10.1016/j.undsp.2019.03.005

Lee YK, Pietruszczak S (2008) A new numerical procedure for elasto-plastic analysis of a circular opening excavated in a strain-softening rock mass. *Tunnelling and Underground Space Technology* 23:588-599, DOI: 10.1016/j.tust.2007.11.002

Mortazavi B, Podryabinkin EV, Roche S, Rabczuk T, Shapeev AV (2020) Machine-learning interatomic potentials enable first-principles multiscale modeling of lattice thermal conductivity in graphene/borophene heterostructures. *Materials Horizons* 7(9):2359-2367, DOI: 10.1039/D0MH00787K

Naghsh MA, Shishegaran A, Karami B, Rabczuk T, Shishegaran A, Taghavizadeh H, Moradi M (2021) An innovative model for predicting the displacement and rotation of column-tree moment connection under fire. *Frontiers of Structural and Civil Engineering* 15(2):1-19, DOI: 10.1007/s11709-020-0688-2

Osgoui RR, Oreste P (2009) Elasto-plastic analytical model for the design of grouted bolts in a Hoek-Brown medium. *International*

Journal for Numerical and Analytical Methods in Geomechanics 34(16):1651-1686, DOI: 10.1002/nag.823

Shishegaran A, Daneshpajoh F, Taghavizade H, Mirvalad S (2020a) Developing conductive concrete containing wire rope and steel powder wastes for route deicing. *Construction and Building Materials* 232:117184, DOI: 10.1016/j.conbuildmat.2019.117184

Shishegaran A, Ghasemi MR,Varaee H (2019) Performance of a novel bent-up bars system not interacting with concrete. *Frontiers of Structural and Civil Engineering* 13:1301-1315, DOI: 10.1007/s11709-019-0552-4

Shishegaran A, Karami B, Rabczuk T, Naghsh MA, Khani MM (2020b) Performance of fixed beam without interacting bars. *Frontiers of Structural and Civil Engineering* 14(5):1180-1195, DOI: 10.1007/s11709-020-0661-0

Shishegaran A, Khalili MR, Karami B, Rabczuk T, Shishegaran A (2020c) Computational predictions for estimating the maximum deflection of reinforced concrete panels subjected to the blast load. *International Journal of Impact Engineering* 139:103527, DOI: 10.1016/j.ijimpeng.2020.103527

Shishegaran A, Saeedi M, Mirvalad S, Korayemd AH (2021a) The mechanical strength of the artificial stones, containing the travertine wastes and sand. *Journal of Materials Research and Technology* 11:1688-1709, DOI: 10.1016/j.jmrt.2021.02.013

Shishegaran A, Varaee H, Rabczuk T, Shishegaran G (2021b) High correlated variables creator machine: Prediction of the compressive strength of concrete. *Computers & Structure* 247:106479, DOI: 10.1016/j.compstruc.2021.106479

Unlu T, Gercek H (2003) Effect of poisson's ratio on the normalized radial displacements occurring around the face of a circular tunnel. *Tunnelling and Underground Space Technology* 18(5):547-553, DOI: 10.1016/S0886-7798(03)00086-5

Zhang CG, Zeng KH (2015) Comparisons and applications of displacement release coefficients for a circular rock tunnel subjected to isotropic geostresses. *Chinese Journal of Rock Mechanics and Engineering* 34(3):498-510, DOI: 10.13722/j.cnki.jrme.2015.03.007 (in Chinese)